

# 1 Lipid droplets fuel SARS-CoV-2 replication and production of 2 inflammatory mediators

3 Suelen da Silva Gomes Dias<sup>1#</sup>, Vinicius Cardoso Soares<sup>1,2#</sup>, André C. Ferreira<sup>1,3,4</sup>,  
4 Carolina Q. Sacramento<sup>1,3</sup>, Natalia Fintelman-Rodrigues<sup>1,3</sup>, Jairo R. Temerozo<sup>5,6</sup>, Livia  
5 Teixeira<sup>1</sup>, Ester Barreto<sup>1</sup>, Mayara Mattos<sup>1,3</sup>, Caroline S. de Freitas<sup>1,3</sup>, Isaclaudia G.  
6 Azevedo-Quintanilha<sup>1</sup>, Pedro Paulo A. Manso<sup>7</sup>, Eugenio D. Hottz<sup>1,8</sup>, Camila R. R. Pão<sup>1</sup>,  
7 Dumith C. Bou-Habib<sup>5,6</sup>, Fernando A. Bozza<sup>9,10</sup>, Thiago M. L. Souza<sup>1,3</sup>, Patrícia T.  
8 Bozza<sup>1\*</sup>

## 9 # - These authors contributed equally to this work

10 1- Laboratory of Immunopharmacology, Oswaldo Cruz Institute (FIOCRUZ), Rio de Janeiro,  
11 RJ, Brazil.

12 2- Program of Immunology and Inflammation, Federal University of Rio de Janeiro, UFRJ, Rio  
13 de Janeiro, RJ, Brazil.

14 3- National Institute for Science and Technology on Innovation on Diseases of Neglected  
15 Populations (INCT/IDNP), Center for Technological Development in Health (CDTS), FIOCRUZ,  
16 Rio de Janeiro, RJ, Brazil.

17 4- Universidade Iguazu, Nova Iguaçu, RJ, Brazil.

18 5- Laboratory on Thymus Research, Oswaldo Cruz Institute (FIOCRUZ), Rio de Janeiro, RJ,  
19 Brazil.

20 6- National Institute for Science and Technology on Neuroimmunomodulation (INCT/NIM),  
21 Oswaldo Cruz Institute, Fiocruz, Rio de Janeiro, RJ, Brazil.

22 7- Laboratory of Patology, Oswaldo Cruz Institute (FIOCRUZ), Rio de Janeiro, RJ, Brazil.

23 8- Laboratory of Immunothrombosis, Department of Biochemistry, Federal University of Juiz de  
24 Fora (UFJF), Juiz de Fora, MG, Brazil;

25 9- National Institute of Infectology (INI), FIOCRUZ, Rio de Janeiro, Brazil.

26 10- D'Or Institute for Research and Education (IDOR), Rio de Janeiro, Brazil.

27 **Keywords:** SARS-CoV-2; COVID-19; Lipid metabolism; Lipid droplet; Pro-inflammatory  
28 cytokines.

29 \*Corresponding author

30 Patrícia T. Bozza

31 [pbozza@ioc.fiocruz.br](mailto:pbozza@ioc.fiocruz.br) or [pbozza@gmail.com](mailto:pbozza@gmail.com)

32 **Abstract**

33 Viruses are obligate intracellular parasites that make use of the host metabolic  
34 machineries to meet their biosynthetic needs, identifying the host pathways essential for  
35 the virus replication may lead to potential targets for therapeutic intervention. The  
36 mechanisms and pathways explored by SARS-CoV-2 to support its replication within  
37 host cells are not fully known. Lipid droplets (LD) are organelles with major functions in  
38 lipid metabolism and energy homeostasis, and have multiple roles in infections and  
39 inflammation. Here we described that monocytes from COVID-19 patients have an  
40 increased LD accumulation compared to SARS-CoV-2 negative donors. *In vitro*, SARS-  
41 CoV-2 infection modulates pathways of lipid synthesis and uptake, including CD36,  
42 SREBP-1, PPAR $\gamma$  and DGAT-1 in monocytes and triggered LD formation in different  
43 human cells. LDs were found in close apposition with SARS-CoV-2 proteins and double-  
44 stranded (ds)-RNA in infected cells. Pharmacological modulation of LD formation by  
45 inhibition of DGAT-1 with A922500 significantly inhibited SARS-CoV-2 replication as  
46 well as reduced production of pro-inflammatory mediators. Taken together, we  
47 demonstrate the essential role of lipid metabolic reprogramming and LD formation in  
48 SARS-CoV-2 replication and pathogenesis, opening new opportunities for therapeutic  
49 strategies to COVID-19.

## 50 **Introduction**

51           The coronavirus disease 2019 (COVID-19) caused by the novel severe acute  
52 respiratory syndrome-coronavirus 2 (SARS-CoV-2) has rapidly spread in a pandemic,  
53 representing an unprecedented health, social and economic threat worldwide (Lu et al.,  
54 2020; Wu et al., 2020). This newly emerged SARS-CoV-2 belongs to the  
55 *Betacoronavirus* genus of the subfamily *Orthocoronavirinae* in the *Coronaviridae*  
56 family. Like other Coronavirus, the SARS-CoV-2 is an enveloped non-segmented  
57 positive-sense RNA (+RNA) virus (Zhu et al., 2020), which genome sequence is similar  
58 to the already known SARS-CoV (Zhou et al., 2020b). Despite the similarity with other  
59 members of the *Betacoronavirus* genus, the pathogenesis of SARS-CoV-2 infection  
60 presents unique properties that contribute to its severity and pandemic-scale spread.  
61 Therefore, it is necessary to understand how the virus interacts and manipulate host cell  
62 metabolism to develop novel strategies to control the clinical progression of the infection  
63 and to limit the SARS-CoV-2 pandemic.

64           Viruses are obligated intracellular pathogens that require host cell machinery to  
65 replicate (Chazal and Gerlier, 2003; Novoa et al., 2005; Takahashi and Suzuki, 2011).  
66 Viruses interact with several intracellular structures and have the ability to reprogram the  
67 cellular metabolism to benefit viral replication (Abrantes et al., 2012; Syed et al., 2010;  
68 Zhang et al., 2017). Accumulated evidence points to major roles of lipid droplets (LD)  
69 for virus replication cycle and pathogenesis, highlighting the potential of these organelles  
70 as targets for drug development. Many studies have demonstrated the interaction of viral  
71 molecules with LD-related components, and the relevance of these organelles for viral  
72 replication as already demonstrated in several positive-strand RNA (+ RNA) viruses such  
73 as *Flaviviridae* members, rotavirus and reovirus (Cheung et al., 2010; Coffey et al., 2006;  
74 Filipe and McLauchlan, 2015; Lyn et al., 2013; Samsa et al., 2009; Villareal et al., 2015).  
75 Accordingly, pharmacological interventions that alter the synthesis of fatty acids,  
76 enzymes associated with lipid metabolism and the formation of LDs reduce viral  
77 replication and assembly (Herker et al., 2010; Martín-Acebes et al., 2011; Villareal et al.,  
78 2015; Yang et al., 2008; Zhang et al., 2017). In addition, LDs play an important role in  
79 the infection pathogenesis and inflammatory processes (Herker and Ott, 2012; Pereira-  
80 Dutra et al., 2019).

81           Here we demonstrate major effects of SARS-CoV-2 to modulate cellular lipid  
82 metabolism in human cells favoring increased de novo lipid synthesis and lipid  
83 remodeling, leading to increased LD accumulation in human cells. We also reported  
84 increased LD accumulation in monocytes from COVID-19 patients when compared to  
85 healthy volunteers. Importantly, the blockade of LD biogenesis with a pharmacological  
86 inhibitor of DGAT-1 decreased viral replication and pro-inflammatory cytokine  
87 production and prevented cell death. Collectively, our results uncover mechanisms of  
88 viral manipulation of host cell lipid metabolism to allow SARS-CoV-2 replication and  
89 may provide new insights for antiviral therapies.

90

## 91 **Results**

### 92 **SARS-CoV-2 infection upregulates lipid metabolism, increasing LD biogenesis in** 93 **human cells.**

94 Viruses have the ability to modulate cellular metabolism with benefits for their  
95 own replication. Several +RNA viruses, including members of *Flaviviridae* family, as  
96 HCV (Boulant et al., 2007; Lyn et al., 2013) and DENV (Carvalho et al., 2012; Samsa et  
97 al., 2009), as well as reovirus (Coffey et al., 2006) and poliovirus (Viktorova et al., 2018)  
98 modify the lipid metabolism in different cells and trigger LD formation, using these host  
99 organelles at different steps of their replicative cycle.

100 Here, we demonstrated increased LD accumulation in human monocytes from  
101 COVID-19 patients when compared with healthy volunteers (Fig. 1A and B). Likewise,  
102 we demonstrated that in vitro infection with SARS-CoV-2 with a multiplicity of infection  
103 (MOI) of 0.01 triggers the increase of LDs in primary human monocytes within 24 hours  
104 (Fig. 1C and D), as well as in a human lung epithelial cell line (A549), and human lung  
105 microvascular endothelial cell line (HMVEC-L) after 48 hours post-infection  
106 (Supplementary Fig. 1).

107 Lipid metabolism alterations in cells and plasma are emerging as major  
108 phenotypes during COVID-19 and SARS-CoV-2 infection (Shen et al., 2020). To gain  
109 insights on the mechanisms involved in LD formation, we evaluated whether SARS-CoV-  
110 2 infection could modulate the expression of the proteins associated with lipid metabolism  
111 involved in lipid uptake and de novo lipid synthesis (Fig. 1E). As shown in figure 1E-G,  
112 SARS-CoV-2 infection of human primary monocytes up-regulated the pathways involved  
113 in lipid uptake such as CD36, the major transcriptional factors involved in lipogenesis,  
114 PPAR $\gamma$  and SREBP-1, and the enzyme DGAT-1, which is involved in triacylglycerol  
115 synthesis, after 24 hours of infection.

116 Altogether, these data suggest that SARS-CoV-2 is able to modulate multiple  
117 pathways of lipid metabolism and remodeling, including in immune cells from COVID-  
118 19 patients, culminating in new LD assembling in human cells.

### 119 **Inhibition of LD formation decreases viral replication and prevents cell death in** 120 **SARS-CoV-2 infected monocytes.**

121 DGAT-1 is a key enzyme involved in the final step of triacylglycerol synthesis  
122 and thus is central to remodel and finish the biogenesis of LDs (Chitraju et al., 2017) .

123 During HCV infection, DGAT-1 was shown to be required for LD biogenesis, and to  
124 control HCV protein trafficking to LDs (Camus et al., 2013). Consequently, DGAT-1  
125 inhibition blocks HCV use of LDs as replication platforms and inhibits viral particle  
126 formation (Camus et al., 2013; Herker et al., 2010). To assess the involvement of DGAT-  
127 1 in LD biogenesis during the SARS-CoV-2 infection, we treated A549 cells with  
128 A922500, an inhibitor of the enzyme DGAT-1, for 2 hours at different concentrations  
129 prior to SARS-CoV-2 infection and evaluated the LD biogenesis 48 hours after infection.  
130 As shown in figure 2A and B, treatment with A922500 inhibited in a dose dependent  
131 manner the LD formation triggered by SARS-CoV-2 infection. Similarly, pre-treatment  
132 with A922500 also blocked LD induced by SARS-CoV-2 in monocytes (Fig. 2A and C).

133 Human monocytes infected with SARS-CoV-2 were shown to sustain viral  
134 genome replication, express higher levels of pro-inflammatory cytokines and may  
135 undergo cell death (Codo et al., 2020). To gain insights on the functions of LDs in SARS-  
136 CoV-2 infection, LD biogenesis was inhibited by A922500, a DGAT-1 inhibitor.  
137 Treatment with A922500 significantly reduced the viral load in human primary  
138 monocytes (Fig. 3A), suggesting a role for DGAT-1 and LD in SARS-CoV-2 replication.

139 It has already been demonstrated the capacity of the SARS-CoV-2 infection to  
140 induce cell death in monocytes, as evidenced by the leak of LDH to the extracellular space  
141 (Fintelman-Rodrigues et al., 2020). Cell death after viral infections can occur due to  
142 changes in cellular homeostasis caused by the virus replication per se and/or by the  
143 heightened inflammatory response. Here, we measured the death of human primary  
144 monocytes infected with SARS-CoV-2 by the release of LDH into the supernatant, and  
145 also by the analysis of cell morphology observed in phase contrast. Our data show that  
146 SARS-CoV-2 triggered increased LDH release in the supernatant and that infected cells  
147 exhibited morphologic alterations with membrane rupture/damage compatible with  
148 necrosis (Fig. 3B and C). Similar to the observed for viral replication, DGAT-1 and LD  
149 inhibition with 10  $\mu$ M of A922500 was able to inhibit SARS-CoV-2-induced cell death  
150 (Fig. 3B and C).

### 151 **Lipid droplets are involved in SARS-CoV-2 heightened inflammatory response**

152 Dysregulated immune response, with increased pro-inflammatory  
153 cytokine/chemokine production is observed during severe COVID-19 and associates with  
154 the outcome of the disease (Coperchini et al., 2020). We observed that primary human  
155 monocytes infected with SARS-CoV-2 exhibit increased production of leukotrienes

156 (LTB<sub>4</sub> and cysLT), pro-inflammatory cytokines (IL-6, TNF $\alpha$  and IL-12) and chemokines  
157 (IL-8 and CXCL10) in comparison with uninfected cells (Fig. 3D, E and F). Regarding  
158 anti-inflammatory mediators, SARS-CoV-2 infection increased IL-10 and reduced IL-4  
159 production in comparison with uninfected monocytes (Fig. 3G).

160 LDs are organelles with major functions in inflammatory mediator production and  
161 innate signaling in immune cells. To evaluate if LDs contribute to SARS-CoV-2-induced  
162 inflammation, monocytes were pre-treated with A922500, the secreted levels of lipid  
163 mediators, cytokine and chemokines were measured 24 h after infection. It has been well  
164 established that LDs are organelles that compartmentalize the eicosanoid synthesis  
165 machinery and are sites for eicosanoid formation (Bozza et al., 2011). Here, we  
166 demonstrated that SARS-CoV-2 infection increased LTB<sub>4</sub> and cysLT production in  
167 comparison with uninfected monocytes (Fig 3D). The pretreatment with DGAT-1  
168 inhibitor A922500 reduced the synthesis of both lipid mediators by infected cells (Fig.  
169 3D). These data point out the importance of LD for the production of these pro-  
170 inflammatory lipid mediators. We also observed that A922500 treatment downregulated  
171 the chemokines IL-8 and CXCL10, and the pro-inflammatory cytokines IL-6, TNF $\alpha$  and  
172 IL-12 (Fig. 3E and F), without affecting the anti-inflammatory cytokine IL-10 (Fig. 3G).  
173 In addition to lowering the pro-inflammatory mediators, inhibition of LDs may shift the  
174 inflammatory profile by increasing the anti-inflammatory cytokine IL-4 (Fig. 3G).

175 Altogether, our data indicate that LDs have important functions in the modulation  
176 of inflammatory mediators production in SARS-CoV-2-infected monocytes and suggest  
177 that LD inhibition may reduce the exaggerated inflammatory process caused by the  
178 cytokine storm.

### 179 **Lipid droplets are sites for SARS-CoV-2 replication.**

180 The up regulation of the lipid metabolism and LD biogenesis by the new SARS-  
181 CoV-2 suggest that the virus may explore host metabolism to favor its replication using  
182 the LDs as a replication platform, as demonstrated for HCV (Boulant et al., 2007; Camus  
183 et al., 2013; Lee et al., 2019) and DENV (Samsa et al., 2009). To evaluate this, we used  
184 a VERO E6 cell line that has a highly replicative capacity.

185 For these experiments, we pre-treated the VERO cells with a range of  
186 concentrations of DGAT-1 inhibitor A922500 (0.1 - 50  $\mu$ M) for 2 hours, followed by  
187 infection with SARS-CoV-2 (MOI 0.01) for 24 hours. The supernatant was used to

188 perform a plaque assay. Here, we observed that A922500 significantly inhibited SARS-  
189 CoV-2 replication in a dose dependent manner with an IC<sub>50</sub> of 3.78  $\mu$ M (Fig. 4A and B).

190 To gain insights on the interaction of the SARS-CoV-2 with LDs we labeled the  
191 virus using immune serum from a convalescent COVID-19 patient that exhibit high anti-  
192 SARS-CoV-2 titers. For that, we stained the LDs using a BODIPY probe and analyzed  
193 the co-localization between the viral proteins and LDs by confocal microscopy. As shown  
194 in figure 4C, intense immunoreactivity (red) was obtained in SARS-CoV-2 infected cells,  
195 whereas no labeling was observed in uninfected cells, indicative of specific SARS-CoV-  
196 2 labeling with COVID-19 convalescent serum (Fig. 4C). As observed for monocytes and  
197 lung cells, Vero E6 infected cells increased LD biogenesis (green). Then, we examined  
198 the spatial relationship between SARS-CoV-2 and LDs. Confocal analysis showed a close  
199 apposition of SARS-CoV-2 immunoreactivity with BODIPY-labeled LDs (red arrows)  
200 and also co-localization of viral protein(s) with BODIPY-labeled LDs (yellow; fuchsia  
201 arrows) in the infected cells (Fig. 4C-D).

202 Accumulating evidence indicate that host LDs play an important role in virus  
203 replicative cycle, including as hubs for viral genome replication and viral particle  
204 assembling (Laufman et al., 2019; Lee et al., 2019; Miyanari et al., 2007; Samsa et al.,  
205 2009) . To assess if LDs are associated with SARS-CoV-2 replication, we use a specific  
206 antibody for double stranded (ds)-RNA (J2 clone). As shown in figure 4E, we observed  
207 strong labeling of the ds-RNA in cells infected with the SARS-CoV-2 compared to  
208 uninfected cells. Similar to labeling detected with convalescent COVID-19 polyclonal  
209 serum, we observed close apposition and/or co-localization between BODIPY-labeled  
210 LDs and ds-RNA (Fig. 4E and E`).

211 Collectively, our data suggest that SARS-CoV-2 uses LDs as a replication  
212 platform, and establish that pharmacological targeting of LD formation inhibit SARS-  
213 CoV-2 replication, emerging as a potential strategy for antiviral development.

214



## 215 Discussion

216 Most positive-strand RNA virus are able to modulate the host lipid metabolism  
217 and to hijack LDs to enhance their fitness and replication/particle assembling capacity  
218 (Herker and Ott, 2012; Pereira-Dutra et al., 2019). The pathways and mechanisms used  
219 may vary according to the virus and the host cell infected. The mechanisms and pathways  
220 explored by SARS-CoV-2 to support its replication within host cells are still largely  
221 unknown. Here we provide evidence that LDs participate at two levels of host pathogen  
222 interaction in SARS-CoV-2 infection: first, they are important players for virus  
223 replication; and second, they are central cell organelles in the amplification of  
224 inflammatory mediator production. First, we demonstrated that SARS-CoV-2 modulates  
225 pathways of lipid uptake and lipogenesis leading to increased LD accumulation in human  
226 host cells. We further showed that LDs are in close proximity with SARS-CoV-2 proteins  
227 and replicating genome, a finding suggestive that LDs are recruited as part of replication  
228 compartment. Second, we showed that inhibition of DGAT-1 blocked LD biogenesis, and  
229 reduced virus replication, cell-death and pro-inflammatory mediator production.

230 LD biogenesis is a multi-mediated and highly coordinated cellular process that  
231 requires new lipid synthesis and/or lipid uptake and remodeling, but the molecular  
232 mechanisms involved in LD formation during inflammation and infection are still not  
233 completely understood. Here, we showed the increased expression of SREBP-1 and the  
234 nuclear receptor PPAR $\gamma$  after SARS-CoV-2 infection indicative of reprogramming of  
235 cells towards a lipogenic phenotype. Accordingly, increased expression of SREBP-1 has  
236 been reported after respiratory viruses including MERS-CoV, SARS-CoV, and shown to  
237 regulate the increase of the LD and the accumulation of the cholesterol during the  
238 infection (Yuan et al., 2019). Consistently, targeting the SREBP-associated lipid  
239 biosynthetic pathways were shown to have antiviral properties (Yuan et al., 2019). The  
240 transcription factor PPAR $\gamma$  is activated by lipid ligands and promotes the expression of  
241 proteins involved in lipid homeostasis and LD biogenesis, and has been implicated in  
242 infectious and non-infectious LD biogenesis in monocytes/macrophages (Almeida et al.,  
243 2014; Souza-Moreira et al., 2019). Based on these data we can suggest that these two  
244 transcription factors are critical for SARS-CoV-2 infection, favoring the lipid synthesis  
245 and LD formation. One important gene up regulated by PPAR $\gamma$  is the membrane receptor  
246 CD36 (Cheng et al., 2016). CD36 plays an important role in the transport and uptake of  
247 long-chain fatty acids into cells and participates in pathological processes, such as

248 metabolic disorders and infections (Febbraio et al., 2001). Previous reports showed that  
249 CD36 levels are increased in HCV and HIV-1 infections (Berre et al., 2013; Meroni et  
250 al., 2005) and that it facilitates the viral attachment on host cell membrane contributing  
251 to viral replication (Cheng et al., 2016). Our results demonstrated that SARS-CoV-2  
252 infection increase the CD36 expression in monocytes, suggesting the increase of lipids  
253 uptake can contribute to LD formation, observed after the infection.

254 Numerous studies established LDs as key organelles during +RNA viruses  
255 replicative cycle (Herker and Ott, 2012). Here, we observed strong labeling of the SARS-  
256 CoV-2 proteins and ds-RNA intimately associated to the LD and in some cases  
257 colocalizing with LD. This fact highly suggests that SARS-CoV-2 recruits LDs to  
258 replication compartments and could use them as building blocks to fuel its own  
259 replication. Indeed, recent studies have shed light on active mechanisms of LD  
260 recruitment to viral replication compartments with bi-directional content exchange and  
261 essential functions to replication and virus particle assembly (Laufman et al., 2019; Lee  
262 et al., 2019).

263 DGAT-1, the key enzyme for triacylglycerol synthesis, is critical for LD  
264 biogenesis and mediate viral protein trafficking to LD by HCV and other viruses.  
265 Moreover, pharmacological suppression of DGAT1 activity inhibits HCV replication at  
266 the assembly step (Camus et al., 2013; Herker et al., 2010). We observed that DGAT-1  
267 expression increases after SARS-CoV-2 infection and that this enzyme can contribute for  
268 the LD remodeling in the host cells. Pharmacological inhibitors of lipid metabolism  
269 protein are able to modulate the LD formation. Therefore, we used the DGAT-1 inhibitor  
270 (A22500) during SARS-CoV-2 infection and observed that this treatment reduced the LD  
271 biogenesis in monocytes and A549 cells, as well as decrease the viral load of SARS-CoV-  
272 2 in monocytes. Importantly, pharmacologically suppressing DGAT1 activity dose  
273 dependently inhibited SARS-CoV-2 infectious particle formation in VERO E6 cells with  
274 an IC<sub>50</sub> of 3.78  $\mu$ M. Thus, suggesting that DGAT-1 activity and LD formation are crucial  
275 to SARS-CoV-2 replication and assembly in these cells.

276 Dysregulated monocyte responses are pivotal in the uncontrolled production of  
277 cytokines during the infection with respiratory viruses, such as influenza A virus (Gao et  
278 al., 2013; Peschke et al., 1993). Dysregulated immune response with key involvement of  
279 monocytes, and increased pro-inflammatory cytokine/chemokine production is also  
280 observed during severe COVID-19 and is associated with the outcome of the disease  
281 (Coperchini et al., 2020; Zhou et al., 2020a). SARS-CoV-2 infection of human monocytes

282 in vitro recapitulate most of the pattern of inflammatory mediator production associated  
283 with COVID-19 severity, including the enhancement of the IL-6 and TNF $\alpha$  levels, and  
284 the consistent cell death, measured by LDH release (Fintelman-Rodrigues et al., 2020;  
285 Temerozo et al., 2020; Zhou et al., 2020a). We showed that SARS-CoV-2 infection  
286 generated a large amount of inflammatory lipid mediators, and cytokine synthesis by  
287 monocytes. Blockage of DGAT-1 activity lead to inhibition of the LDs and significantly  
288 reduced leukotriene production and pro-inflammatory cytokines released by monocytes,  
289 suggesting an important role for LDs to control the inflammatory process, and  
290 consequently to prevent the cell death-related with the uncontrolled inflammation. This  
291 finding is in agreement with the well-established role of LDs in inflammation and innate  
292 immunity (Bozza and Viola, 2010; Pereira-Dutra et al., 2019). Therefore, our data support  
293 a role for LD in the heightened inflammatory production triggered by SARS-CoV-2 and  
294 conversely, inhibition of LD biogenesis by targeting DGAT1 activity may have beneficial  
295 effects on disease pathogenesis.

296 In summary, our data demonstrate that SARS-CoV-2 triggers reprogramming of  
297 lipid metabolism in monocytes and other cells leading to accumulation of LDs favoring  
298 virus replication. The inhibition of LD biogenesis modulates the viral replication and the  
299 pro-inflammatory mediator production. Therefore, our data support the hypothesis that  
300 SARS-CoV-2 infection increases the expression of the lipid metabolism-related proteins  
301 for their own benefit towards replication and fitness. Although, further studies are  
302 certainly necessary to better characterize the full mechanisms and importance of the LDs  
303 during the SARS-CoV-2 infection, our findings support major roles for LDs in SARS-  
304 CoV-2 replicative cycle and immune response. Moreover, the finding that the host lipid  
305 metabolism and LDs are required for SARS-CoV-2 replication suggests a potential  
306 strategy to interfere with SARS-CoV-2 replication by blocking the DGAT1 and other  
307 lipid metabolic pathway enzymes.

308

309 **Acknowledgments**

310 We thank the Hemotherapy Service from Hospital Clementino Fraga Filho  
311 (Federal University of Rio de Janeiro, Brazil) for providing buffy-coats. The authors  
312 thank the confocal imaging facility from the Rede de Plataformas Tecnológicas  
313 FIOCRUZ and Dr. Carmen Beatriz Wagner Giacoia Gripp for assessments related to  
314 BSL3 facility. This work was supported by grants from Inova program Fiocruz, Fundação  
315 de Amparo à Pesquisa do Estado do Rio de Janeiro (FAPERJ), Conselho Nacional de  
316 Desenvolvimento Científico e Tecnológico (CNPq) and Coordenação de  
317 Aperfeiçoamento de Pessoal de Nível Superior (CAPES) granted for Patrícia T. Bozza,  
318 Thiago Moreno L. Souza, Dumith Chequer Bou-Habib and Fernando A. Bozza.

319 **Author Contribution.**

320 Conceived the study: SSGD, VCS, FAB, TMLS, PTB; Designed the experiments: SSGD,  
321 VCS, TMLS; PTB; Performed the experiments: SSGD, VCS, ACF, CQS, NFR, JRT, LT,  
322 EB, MM, CSF, IGAQ, PPM, EH, CRRP; Analyzed the data: SSGD, VCS, DCBH, TMLS,  
323 PTB; Wrote the paper: SSGD, VCS, TMLS, PTB. All authors reviewed and approved the  
324 manuscript.

325 The authors declare no competing financial interests.

326

327

## 328 **Methodology**

329 **Cells, virus and reagents.** Blood were obtained from RT-PCR-confirmed COVID-19  
330 patients and SARS-CoV-2-negative health volunteers. Human monocytes were isolated  
331 from peripheral blood mononuclear cells (PBMCs) using density gradient centrifugation  
332 (Ficoll-Paque, GE Healthcare). The PBMC were resuspended in PBS containing 1 mM  
333 EDTA and 2 % fetal bovine serum (FBS; GIBCO) to the concentration of  $10^8$  cells/mL.  
334 The cells were incubated with anti-CD14 antibodies (1:10) for 10 min and magnetic  
335 beads-conjugates (1:20) for additional 10 min, followed by magnetic recovery of  
336 monocytes for 5 min. Recovered monocytes were resuspended in PBS containing 1 mM  
337 EDTA and 2 % FBS and subjected to two more rounds of selection in the magnet  
338 according to the manufacturer's instructions (Human CD14+ selection kit, Easy Sep;  
339 StemCell). The purity of monocyte preparations (>98% CD14+ cells) was confirmed  
340 through flow cytometry.

341 Human primary monocyte was obtained through plastic adherence of PBMCs. Briefly,  
342 PBMCs were isolated by Ficoll-Paque from peripheral blood or from buff-coat  
343 preparations of healthy donors. PBMCs ( $2 \times 10^6$ ) were plated onto 48-well plates in low  
344 glucose Dulbecco's modified Eagle's medium (DMEM; GIBCO). After 2 hours of the  
345 plaque, non-adherent cells were washed out and the remaining monocytes were  
346 maintained for 24 hours in DMEM containing 5% inactivated male human AB serum  
347 (HS; Merck) and 100 U/mL penicillin-streptomycin (P/S; GIBCO) at 37 °C in 5 % CO<sub>2</sub>.  
348 The purity of human monocytes was above 90 %, as analyzed by flow cytometry analysis  
349 (FACScan; Becton Dickinson) using anti-CD3 (BD Biosciences) and anti-CD16  
350 (Southern Biotech) monoclonal antibodies.

351 Human lung epithelial carcinoma cell line (A549 - ATCC/CCL-185) and African green  
352 monkey kidney (Vero subtype E6) were cultured in high glucose DMEM supplemented  
353 with 10% FBS and 100 U/mL P/S, and were incubated at 37 °C in 5 % CO<sub>2</sub>.

354 Human lung microvascular endothelial cell line (HMVEC-L - LONZA/CC-2527) was  
355 maintained following the manufacturer's instructions. The cells were cultured in  
356 endothelial growth medium (EGM<sup>TM</sup>-2MV BulletKit<sup>TM</sup>, Clonetics) supplemented with 5  
357 % fetal bovine serum (FBS, Clonetics) and cells were incubated at 37 °C and 5 % CO<sub>2</sub>.

358 SARS-CoV-2 was originally isolated from nasopharyngeal swabs of confirmed case from  
359 Rio de Janeiro/Brazil (GenBank accession no. MT710714). The virus was amplified in  
360 Vero E6 cells in high glucose DMEM supplemented with 2% FBS, incubated at 37°C in  
361 5% CO<sub>2</sub> during 2 to 4 days of infection. Virus titers were performed by the tissue culture  
362 infectious dose at 50% (TCID<sub>50</sub>/mL) and the virus stocks kept in -80 °C freezers.  
363 According to WHO guidelines, all procedures involving virus culture were performed in  
364 biosafety level 3 (BSL3) multiuser facility.

365 **Infections and virus titration.** After 24h of cell plating, the SARS-CoV-2 infections  
366 were performed at MOI of 0.01 in all cells with or without pre-treatment with the  
367 pharmacological inhibitor of DGAT-1 (A922500 – Sigma CAS 959122-11-3) for two  
368 hours. The Plaque-forming Assay was performed for virus titration in VERO E6 cells  
369 seeded in 24-well plates. Cell monolayers were infected with different dilutions of the  
370 supernatant containing the virus for 1h at 37°C. The cells were overlaid with high glucose  
371 DMEM containing 2% FBS and 2.4% carboxymethylcellulose. After 3 days, the cells  
372 were fixed with 10% formaldehyde in PBS for 3h. The cell monolayers were stained with  
373 0.04% crystal violet in 20% ethanol for 1h. The viral titer was calculated from the count  
374 of plaques formed in the wells corresponding to each dilution and expressed as plaque  
375 forming unit per mL (PFU/mL).

376

377 **Lipid droplet staining.** Human primary monocytes, A549 cell line, and HMVEC cell  
378 line were seeded in coverslips. The cells infected or not were fixed using 3.7%  
379 formaldehyde. In addition, after isolation, the monocytes from COVID-19 patients were  
380 fixed using 3.7% formaldehyde and adhered in coverslips through cytospin (500 x g for  
381 5 min). The LDs were stained with 0.3% Oil Red O (diluted in 60% isopropanol) for  
382 2 min at room temperature. The coverslips were mounted in slides using an antifade  
383 mounting medium (VECTASHIELD®). Nuclear recognition was based on DAPI staining  
384 (1 µg/mL) for 5 min. Fluorescence was analyzed by fluorescence microscopy with an  
385 100x objective lens (Olympus, Tokyo, Japan). The numbers of LDs were automatically  
386 quantified by ImageJ software analysis from 15 aleatory fields.

387

388 **Immunofluorescence staining.** VERO E6 cells were seeded in coverslips and after 48h  
389 were fixed using 3.7% formaldehyde. Cells were rinsed three times with PBS containing  
390 0.1 M CaCl<sub>2</sub> and 1 M MgCl<sub>2</sub> (PBS/CM) and then permeabilized with 0.1% Triton X-100

391 plus 0.2% BSA in PBS/CM for 10 min (PBS/CM/TB). Cells were stained with  
392 convalescent serum from a patient to identify with COVID-19 at 1:500 dilution for  
393 overnight, followed by a human anti-IgG-Alexa 546 at 1:1000 dilution for 1 h. The  
394 double-RNA was labeling by mouse monoclonal antibody J2 clone - Scicons (Schönborn  
395 et al., 1991) at 1:500 dilution for overnight, followed by a mouse anti-IgG-Dylight 550  
396 at 1:1000 dilution for 1h. LDs were stained with BODIPY493/503 dye (dilution 1:5000  
397 in water) for 5 min. The coverslips were mounted in slides using an antifade mounting  
398 medium (VECTASHIELD®). Nuclear recognition was based on DAPI staining  
399 (1 µg/mL) for 5 min. Fluorescence was analyzed by fluorescence microscopy with an  
400 100x objective lens (Olympus, Tokyo, Japan) or Confocal Microscopy (Laser scanning  
401 microscopy LSM710 Meta, Zeiss).

402 **SDS-PAGE and Western blot.** After 24h of SARS-CoV-2 infection, monocytes were  
403 harvested using ice-cold lysis buffer (1% Triton X-100, 2% SDS, 150 mM NaCl, 10 mM  
404 HEPES, 2 mM EDTA containing protease inhibitor cocktail - Roche). Cell lysates were  
405 heated at 100 °C for 5 min in the presence of Laemmli buffer (20% β-mercaptoethanol;  
406 370 mM Tris base; 160 µM bromophenol blue; 6% glycerol; 16% SDS; pH 6.8).  
407 Twenty µg of protein/sample were resolved by electrophoresis on SDS-containing 10%  
408 polyacrylamide gel (SDS-PAGE). After electrophoresis, the separated proteins were  
409 transferred to nitrocellulose membranes and incubated in blocking buffer (5% nonfat  
410 milk, 50 mM Tris-HCl, 150 mM NaCl, and 0.1% Tween 20). Membranes were probed  
411 overnight with the following antibodies: anti-PPAR $\gamma$  (Santa Cruz Biotechnology, #SC-  
412 7196 - H100), anti-CD36 (Proteintech-18836-1-AP), anti-SREBP-1 (Ab-28481), anti-  
413 DGAT-1 (Santa Cruz Biotechnology, #SC-271934) and anti-β-actin (Sigma, #A1978).  
414 After the washing steps, they were incubated with IRDye - LICOR or HRP-conjugated  
415 secondary antibodies. All antibodies were diluted in blocking buffer. The detections were  
416 performed by Supersignal Chemiluminescence (GE Healthcare) or by fluorescence  
417 imaging using the Odyssey system. The densitometries were analyzed using the Image  
418 Studio Lite Ver 5.2 software.

419 **Measurement of viral RNA load.** Supernatants from monocytes were harvested after  
420 24h of SARS-CoV-2 infection and the viral RNA quantified through RT-PCR. According  
421 to manufacturer's protocols, the total RNA from each sample was extracted using QIAamp  
422 Viral RNA (Qiagen®). Quantitative RT-PCR was performed using QuantiTect Probe RT-  
423 PCR Kit (Qiagen®) in a StepOne™ Real-Time PCR System (Thermo Fisher Scientific).

424 Amplifications were carried out containing 2× reaction mix buffer, 50 μM of each primer,  
425 10 μM of probe, and 5 μL of RNA template in 15 μL reaction mixtures. Primers, probes,  
426 and cycling conditions recommended by the Centers for Disease Control and Prevention  
427 (CDC) protocol were used to detect the SARS-CoV-2 (CDC, 2020). For virus  
428 quantification it was employed the standard curve method. Cells of each sample were  
429 counted before the PCR analyses for normalization. The Ct values for this target were  
430 compared to those obtained to different cell amounts, 10<sup>7</sup> to 10<sup>2</sup>, for calibration.

431 **Measurements of inflammatory mediators and LDH activity.** The monocyte  
432 supernatant was obtained after 24 hours of SARS-CoV-2 infection with or without pre-  
433 treatment with A922500 (10 μM). Cytokines and chemokines were measured in the  
434 supernatant by ELISA following the manufacturer's instructions (Duo set, R&D). LTB<sub>4</sub>  
435 and cysLT were measured in the supernatant by EIA following the manufacturer's  
436 instructions (Cayman Chemicals). Cell death was determined according to the activity of  
437 lactate dehydrogenase (LDH) in the culture supernatants using a CytoTox® Kit according  
438 to the manufacturer's instructions (Promega, USA).

439 **Ethics statement.** Experimental procedures involving human cells from healthy donors  
440 were performed with samples obtained after written informed consent and were approved  
441 by the Institutional Review Board (IRB) of the Oswaldo Cruz Foundation/Fiocruz (Rio  
442 de Janeiro, RJ, Brazil) under the number 397-07. Experimental procedures involving  
443 human patient cells were performed with samples obtained after written informed consent  
444 from all participants or patients' representatives according to the study protocol approved  
445 by the National Review Board (CONEP 30650420.4.1001.0008).

446 **Statistical analysis.** Data are expressed as mean ± standard error of the mean (SEM) at  
447 least of three and maximum of five independent healthy donors. The paired two-tailed *t*-  
448 test was used to evaluate the significance of the two groups. Multiple comparisons among  
449 three or more groups were performed by one-way ANOVA followed by Tukey's multiple  
450 comparison test. *p* values < 0.05 were considered statistically significant when compared  
451 SARS-CoV-2 infection to the uninfected control (\*) group or SARS-CoV-2 infection  
452 with A922500 treat group (#).



## 453 **Figure Legends**

### 454 **Fig 1. SARS-CoV-2 infection modulates the lipid metabolism in human monocytes.**

455 (A and C) LDs were captured by fluorescent microscopy after Oil Red O staining (Red)  
456 and nuclei stained with DAPI (Blue). (A) Representative images of monocytes from  
457 COVID-19 patients and health volunteers. (C) Representative images of human  
458 monocytes obtained from PBMC infected by SARS-CoV-2 with MOI of 0.01 for 24  
459 hours. Scale bar 20 $\mu$ m. (B and D) LDs were evaluated by ImageJ software analysis by  
460 the measurement of the fluorescent area. (E) Representative scheme of the increase of  
461 proteins associated with lipid metabolism by SARS-CoV-2 infection in monocyte can  
462 regulate the lipid droplet formation. (F) Monocytes were infected by SARS-CoV-2 with  
463 MOI of 0.01 during 24h. Cell lysates were collected for the detection of CD36, PPAR- $\gamma$ ,  
464 SREBP-1, DGAT-1 by Western blotting.  $\beta$ -actin level were used for control of protein  
465 loading. (G) Densitometry data set of each protein. Data are expressed as mean  $\pm$  SEM  
466 of five healthy volunteers (HV) for ex vivo experiments and three healthy donors for LDs  
467 staining and western blot. \* $p < 0.05$  versus health volunteers or uninfected cells.

### 468 **Fig 2. The A922500 inhibits lipid droplet biogenesis induced by SARS-CoV-2 in** 469 **human pulmonary cells and monocytes.**

470 Human pulmonary cell (A549 cell line) and monocytes were pre-treated with DGAT-1  
471 inhibitor A922500 for 2 hours before the infection with SARS-CoV-2 at MOI of 0.01  
472 during 24h in monocytes and 48h in A549 cell line. (A) LDs were captured by fluorescent  
473 microscopy after Oil Red O staining (Red) and nuclei stained with DAPI (Blue). Scale  
474 bar 20 $\mu$ m. (B and C) LDs were evaluated by ImageJ software analysis by the  
475 measurement of the fluorescent area of (B) A549 pre-treated with A922500 using  
476 different concentrations (0.1, 1 and 10 $\mu$ M) and (C) LDs from monocytes pre-treated with  
477 A922500 (10 $\mu$ M). Data are expressed as mean  $\pm$  SEM obtained in four independent  
478 experiments or donors. \* $p < 0.05$  versus uninfected cells and # $p < 0.05$  versus A922500  
479 treated cells.

### 480 **Fig 3. Inhibitor A922500 decreases the pro-inflammatory profile and cell death** 481 **induced by SARS-CoV-2 infection and reduces the viral load in human monocyte.**

482 Monocytes were pre-treated with DGAT-1 inhibitor A922500 (10 $\mu$ M) for 2 hours before  
483 the infection with SARS-CoV-2 with MOI of 0.01 during 24h. (A) Cell death was  
484 measured in the supernatant by LDH activity fold change in relation to the uninfected  
485 cell. (B) Viral load by qPCR. Monocytes of each sample were counted for normalization.  
486 (C) Images of phase contrast from monocytes. Scale bar 20 $\mu$ m. (D-G) The inflammatory  
487 cytokines were measured in supernatants by ELISA (D) leukotrienes: CysLT and LTB<sub>4</sub>,  
488 (E) chemokines: IL-8 and CXCL-10, (F) pro-inflammatory: IL-6, TNF- $\alpha$  and IL-12 and  
489 (G) anti-inflammatory cytokines: IL-10 and IL-4. Data are expressed as mean  $\pm$  SEM  
490 obtained in four independent donors. \*  $p < 0.05$  versus uninfected cells and # $p < 0.05$   
491 versus A922500 treated cells.

### 492 **Fig 4. Lipid droplets is necessary for SARS-CoV-2 replication in VERO E6.**

493 VERO E6 were pre-treated with DGAT-1 inhibitor A922500 with different  
494 concentrations (0.1, 1, 10 and 50 $\mu$ M) for 2 hours before the infection with SARS-CoV-2  
495 with MOI of 0.01 for 24h. (A) Viral replication was determinate by Plaque assay. (B)  
496 Representative Plaque assay. (C-E) Immunofluorescence analyses of VERO E6 after  
497 SARS-CoV-2 infection with MOI of 0.01 for 48h. (C) The virus was detected by indirect  
498 immunofluorescence using convalescent donor serum (Red or white) or (E) the double  
499 strain RNA was detected by indirect immunofluorescence by J2 antibody (Red), the lipid  
500 droplets were stained with BODIPY 493/503 (Green) and nuclei stained with DAPI  
501 (Blue). (C' and E') Representative zoom images. Data are expressed of four independent  
502 experiments for SARS-CoV-2 replication and three for immunofluorescent analyse. #p  
503 <0.05 versus A922500 treated cells. Scale bar 20 $\mu$ m.

504 **Fig S1. SARS-CoV-2 induces an increase of the LD biogenesis in different human**  
505 **pulmonary cell lines.**

506 Human pulmonary cell lines were infected with SARS-CoV-2 at MOI of 0.01 for 48h. (A  
507 and C) LDs were captured by fluorescent microscopy after Oil Red O staining (Red) and  
508 nuclei stained with DAPI (Blue). (B and D) LDs were evaluated by ImageJ software  
509 analysis by the measurement of the fluorescent area. Data are expressed of three  
510 independent experiments. \*p <0.05 versus uninfected cells. Scale bar 20 $\mu$ m.

511

512

## 513 **References**

- 514 Abrantes, J.L., Alves, C.M., Costa, J., Almeida, F.C., Sola-Penna, M., Fontes, C.F., and Souza,  
515 T.M. (2012). Herpes simplex type 1 activates glycolysis through engagement of the enzyme 6-  
516 phosphofructo-1-kinase (PFK-1). *Biochim Biophys Acta* 1822, 1198-1206.
- 517 Almeida, P.E., Roque, N.R., Magalhaes, K.G., Mattos, K.A., Teixeira, L., Maya-Monteiro, C.,  
518 Almeida, C.J., Castro-Faria-Neto, H.C., Ryffel, B., Quesniaux, V.F., *et al.* (2014). Differential  
519 TLR2 downstream signaling regulates lipid metabolism and cytokine production triggered by  
520 *Mycobacterium bovis* BCG infection. *Biochim Biophys Acta* 1841, 97-107.
- 521 Berre, S., Gaudin, R., Cunha de Alencar, B., Desdouits, M., Chabaud, M., Naffakh, N., Rabaza-  
522 Gairi, M., Gobert, F.X., Jouve, M., and Benaroch, P. (2013). CD36-specific antibodies block  
523 release of HIV-1 from infected primary macrophages and its transmission to T cells. *J Exp Med*  
524 210, 2523-2538.
- 525 Boulant, S., Targett-Adams, P., and McLauchlan, J. (2007). Disrupting the association of hepatitis  
526 C virus core protein with lipid droplets correlates with a loss in production of infectious virus. *J*  
527 *Gen Virol* 88, 2204-2213.
- 528 Bozza, P.T., Bakker-Abreu, I., Navarro-Xavier, R.A., and Bandeira-Melo, C. (2011). Lipid body  
529 function in eicosanoid synthesis: an update. *Prostaglandins Leukot Essent Fatty Acids* 85, 205-  
530 213.
- 531 Bozza, P.T., and Viola, J.P. (2010). Lipid droplets in inflammation and cancer. *Prostaglandins*  
532 *Leukot Essent Fatty Acids* 82, 243-250.
- 533 Camus, G., Herker, E., Modi, A.A., Haas, J.T., Ramage, H.R., Farese, R.V., and Ott, M. (2013).  
534 Diacylglycerol acyltransferase-1 localizes hepatitis C virus NS5A protein to lipid droplets and  
535 enhances NS5A interaction with the viral capsid core. *J Biol Chem* 288, 9915-9923.
- 536 Carvalho, F.A., Carneiro, F.A., Martins, I.C., Assuncao-Miranda, I., Faustino, A.F., Pereira,  
537 R.M., Bozza, P.T., Castanho, M.A., Mohana-Borges, R., Da Poian, A.T., *et al.* (2012). Dengue  
538 virus capsid protein binding to hepatic lipid droplets (LD) is potassium ion dependent and is  
539 mediated by LD surface proteins. *J Virol* 86, 2096-2108.
- 540 CDC (2020). Centers for Disease Control and Prevention, Coronavirus Disease 2019 (COVID-  
541 19) (<https://www.cdc.gov/coronavirus/2019-ncov/lab/rt-pcr-panel-primerprobes.html>).
- 542 Chazal, N., and Gerlier, D. (2003). Virus entry, assembly, budding, and membrane rafts.  
543 *Microbiol Mol Biol Rev* 67, 226-237, table of contents.
- 544 Cheng, J.J., Li, J.R., Huang, M.H., Ma, L.L., Wu, Z.Y., Jiang, C.C., Li, W.J., Li, Y.H., Han, Y.X.,  
545 Li, H., *et al.* (2016). CD36 is a co-receptor for hepatitis C virus E1 protein attachment. *Sci Rep*  
546 6, 21808.
- 547 Cheung, W., Gill, M., Esposito, A., Kaminski, C.F., Courousse, N., Chwetzoff, S., Trugnan, G.,  
548 Keshavan, N., Lever, A., and Desselberger, U. (2010). Rotaviruses associate with cellular lipid  
549 droplet components to replicate in viroplasms, and compounds disrupting or blocking lipid  
550 droplets inhibit viroplasm formation and viral replication. *J Virol* 84, 6782-6798.
- 551 Chitraju, C., Mejhert, N., Haas, J.T., Diaz-Ramirez, L.G., Grueter, C.A., Imbriglio, J.E., Pinto,  
552 S., Koliwad, S.K., Walther, T.C., and Farese, R.V. (2017). Triglyceride Synthesis by DGAT1  
553 Protects Adipocytes from Lipid-Induced ER Stress during Lipolysis. *Cell Metab* 26, 407-  
554 418.e403.
- 555 Codo, A.C., Davanzo, G.G., Monteiro, L.B., de Souza, G.F., Muraro, S.P., Virgilio-da-Silva, J.V.,  
556 Prodonoff, J.S., Carregari, V.C., de Biagi Junior, C.A.O., Crunfli, F., *et al.* (2020). Elevated  
557 Glucose Levels Favor SARS-CoV-2 Infection and Monocyte Response through a HIF-  
558 1 $\alpha$ /Glycolysis-Dependent Axis. *Cell Metab*.
- 559 Coffey, C.M., Sheh, A., Kim, I.S., Chandran, K., Nibert, M.L., and Parker, J.S. (2006). Reovirus  
560 outer capsid protein micro1 induces apoptosis and associates with lipid droplets, endoplasmic  
561 reticulum, and mitochondria. *J Virol* 80, 8422-8438.

562 Coperchini, F., Chiovato, L., Croce, L., Magri, F., and Rotondi, M. (2020). The cytokine storm  
563 in COVID-19: An overview of the involvement of the chemokine/chemokine-receptor system.  
564 *Cytokine Growth Factor Rev* 53, 25-32.

565 Febbraio, M., Hajjar, D.P., and Silverstein, R.L. (2001). CD36: a class B scavenger receptor  
566 involved in angiogenesis, atherosclerosis, inflammation, and lipid metabolism. *J Clin Invest* 108,  
567 785-791.

568 Filipe, A., and McLauchlan, J. (2015). Hepatitis C virus and lipid droplets: finding a niche. *Trends*  
569 *Mol Med* 21, 34-42.

570 Fintelman-Rodrigues, N., Sacramento, C.Q., Lima, C.R., da Silva, F.S., Ferreira, A.C., Mattos,  
571 M., de Freitas, C.S., Soares, V.C., Gomes Dias, S.d.S., Temerozo, J.R., *et al.* (2020). Atazanavir  
572 inhibits SARS-CoV-2 replication and pro-inflammatory cytokine production. *bioRxiv*,  
573 2020.2004.2004.020925.

574 Gao, R., Bhatnagar, J., Blau, D.M., Greer, P., Rollin, D.C., Denison, A.M., Deleon-Carnes, M.,  
575 Shieh, W.J., Sambhara, S., Tumpey, T.M., *et al.* (2013). Cytokine and chemokine profiles in lung  
576 tissues from fatal cases of 2009 pandemic influenza A (H1N1): role of the host immune response  
577 in pathogenesis. *Am J Pathol* 183, 1258-1268.

578 Herker, E., Harris, C., Hernandez, C., Carpentier, A., Kaehlcke, K., Rosenberg, A.R., Farese,  
579 R.V., and Ott, M. (2010). Efficient hepatitis C virus particle formation requires diacylglycerol  
580 acyltransferase-1. *Nat Med* 16, 1295-1298.

581 Herker, E., and Ott, M. (2012). Emerging role of lipid droplets in host/pathogen interactions. *J*  
582 *Biol Chem* 287, 2280-2287.

583 Laufman, O., Perrino, J., and Andino, R. (2019). Viral Generated Inter-Organelle Contacts  
584 Redirect Lipid Flux for Genome Replication. *Cell* 178, 275-289.e216.

585 Lee, J.Y., Cortese, M., Haselmann, U., Tabata, K., Romero-Brey, I., Funaya, C., Schieber, N.L.,  
586 Qiang, Y., Bartenschlager, M., Kallis, S., *et al.* (2019). Spatiotemporal Coupling of the Hepatitis  
587 C Virus Replication Cycle by Creating a Lipid Droplet- Proximal Membranous Replication  
588 Compartment. *Cell Rep* 27, 3602-3617.e3605.

589 Lu, R., Zhao, X., Li, J., Niu, P., Yang, B., Wu, H., Wang, W., Song, H., Huang, B., Zhu, N., *et*  
590 *al.* (2020). Genomic characterisation and epidemiology of 2019 novel coronavirus: implications  
591 for virus origins and receptor binding. *Lancet* 395, 565-574.

592 Lyn, R.K., Hope, G., Sherratt, A.R., McLauchlan, J., and Pezacki, J.P. (2013). Bidirectional lipid  
593 droplet velocities are controlled by differential binding strengths of HCV core DII protein. *PLoS*  
594 *One* 8, e78065.

595 Martín-Acebes, M.A., Blázquez, A.B., Jiménez de Oya, N., Escribano-Romero, E., and Saiz, J.C.  
596 (2011). West Nile virus replication requires fatty acid synthesis but is independent on  
597 phosphatidylinositol-4-phosphate lipids. *PLoS One* 6, e24970.

598 Meroni, L., Giacomet, V., Morelli, P., Erba, P., Galazzi, M., Riva, A., Viganò, A., and Galli, M.  
599 (2005). Increased CD36 expression in vertically human immunodeficiency virus-infected  
600 children unrelated to antiretroviral therapy. *Pediatr Infect Dis J* 24, 576-577.

601 Miyanari, Y., Atsuzawa, K., Usuda, N., Watashi, K., Hishiki, T., Zayas, M., Bartenschlager, R.,  
602 Wakita, T., Hijikata, M., and Shimotohno, K. (2007). The lipid droplet is an important organelle  
603 for hepatitis C virus production. *Nat Cell Biol* 9, 1089-1097.

604 Novoa, R.R., Calderita, G., Arranz, R., Fontana, J., Granzow, H., and Risco, C. (2005). Virus  
605 factories: associations of cell organelles for viral replication and morphogenesis. *Biol Cell* 97,  
606 147-172.

607 Pereira-Dutra, F.S., Teixeira, L., de Souza Costa, M.F., and Bozza, P.T. (2019). Fat, fight, and  
608 beyond: The multiple roles of lipid droplets in infections and inflammation. *J Leukoc Biol* 106,  
609 563-580.

610 Peschke, T., Bender, A., Nain, M., and Gems, D. (1993). Role of macrophage cytokines in  
611 influenza A virus infections. *Immunobiology* 189, 340-355.

612 Samsa, M.M., Mondotte, J.A., Iglesias, N.G., Assuncao-Miranda, I., Barbosa-Lima, G., Da Poian,  
613 A.T., Bozza, P.T., and Gamarnik, A.V. (2009). Dengue virus capsid protein usurps lipid droplets  
614 for viral particle formation. *PLoS Pathog* 5, e1000632.

- 615 Schönborn, J., Oberstrass, J., Breyel, E., Tittgen, J., Schumacher, J., and Lukacs, N. (1991).  
616 Monoclonal antibodies to double-stranded RNA as probes of RNA structure in crude nucleic acid  
617 extracts. *Nucleic Acids Res* *19*, 2993-3000.
- 618 Shen, B., Yi, X., Sun, Y., Bi, X., Du, J., Zhang, C., Quan, S., Zhang, F., Sun, R., Qian, L., *et al.*  
619 (2020). Proteomic and Metabolomic Characterization of COVID-19 Patient Sera. *Cell* *182*, 59-  
620 72.e15.
- 621 Souza-Moreira, L., Soares, V.C., Dias, S.D.S.G., and Bozza, P.T. (2019). Adipose-derived  
622 Mesenchymal Stromal Cells Modulate Lipid Metabolism and Lipid Droplet Biogenesis via  
623 AKT/mTOR -PPAR $\gamma$  Signalling in Macrophages. *Sci Rep* *9*, 20304.
- 624 Syed, G.H., Amako, Y., and Siddiqui, A. (2010). Hepatitis C virus hijacks host lipid metabolism.  
625 *Trends Endocrinol Metab* *21*, 33-40.
- 626 Takahashi, T., and Suzuki, T. (2011). Function of membrane rafts in viral lifecycles and host  
627 cellular response. *Biochem Res Int* *2011*, 245090.
- 628 Temerozo, J.R., Sacramento, C.Q., Fintelman-Rodrigues, N., Pão, C.R.R., de Freitas, C.S., da  
629 Silva Gomes Dias, S., Ferreira, A.C., Mattos, M., Soares, V.C., Teixeira, L., *et al.* (2020). The  
630 neuropeptides VIP and PACAP inhibit SARS-CoV-2 replication in monocytes and lung epithelial  
631 cells, decrease the production of proinflammatory cytokines, and VIP levels are associated with  
632 survival in severe Covid-19 patients. *bioRxiv*, 2020.2007.2025.220806.
- 633 Viktorova, E.G., Nchoutmboube, J.A., Ford-Siltz, L.A., Iverson, E., and Belov, G.A. (2018).  
634 Phospholipid synthesis fueled by lipid droplets drives the structural development of poliovirus  
635 replication organelles. *PLoS Pathog* *14*, e1007280.
- 636 Villareal, V.A., Rodgers, M.A., Costello, D.A., and Yang, P.L. (2015). Targeting host lipid  
637 synthesis and metabolism to inhibit dengue and hepatitis C viruses. *Antiviral Res* *124*, 110-121.
- 638 Wu, F., Zhao, S., Yu, B., Chen, Y.M., Wang, W., Song, Z.G., Hu, Y., Tao, Z.W., Tian, J.H., Pei,  
639 Y.Y., *et al.* (2020). A new coronavirus associated with human respiratory disease in China. *Nature*  
640 *579*, 265-269.
- 641 Yang, W., Hood, B.L., Chadwick, S.L., Liu, S., Watkins, S.C., Luo, G., Conrads, T.P., and Wang,  
642 T. (2008). Fatty acid synthase is up-regulated during hepatitis C virus infection and regulates  
643 hepatitis C virus entry and production. *Hepatology* *48*, 1396-1403.
- 644 Yuan, S., Chu, H., Chan, J.F., Ye, Z.W., Wen, L., Yan, B., Lai, P.M., Tee, K.M., Huang, J., Chen,  
645 D., *et al.* (2019). SREBP-dependent lipidomic reprogramming as a broad-spectrum antiviral  
646 target. *Nat Commun* *10*, 120.
- 647 Zhang, J., Lan, Y., and Sanyal, S. (2017). Modulation of Lipid Droplet Metabolism-A Potential  
648 Target for Therapeutic Intervention in. *Front Microbiol* *8*, 2286.
- 649 Zhou, F., Yu, T., Du, R., Fan, G., Liu, Y., Liu, Z., Xiang, J., Wang, Y., Song, B., Gu, X., *et al.*  
650 (2020a). Clinical course and risk factors for mortality of adult inpatients with COVID-19 in  
651 Wuhan, China: a retrospective cohort study. *Lancet* *395*, 1054-1062.
- 652 Zhou, P., Yang, X.L., Wang, X.G., Hu, B., Zhang, L., Zhang, W., Si, H.R., Zhu, Y., Li, B., Huang,  
653 C.L., *et al.* (2020b). A pneumonia outbreak associated with a new coronavirus of probable bat  
654 origin. *Nature* *579*, 270-273.
- 655 Zhu, N., Zhang, D., Wang, W., Li, X., Yang, B., Song, J., Zhao, X., Huang, B., Shi, W., Lu, R.,  
656 *et al.* (2020). A Novel Coronavirus from Patients with Pneumonia in China, 2019. *N Engl J Med*  
657 *382*, 727-733.

658

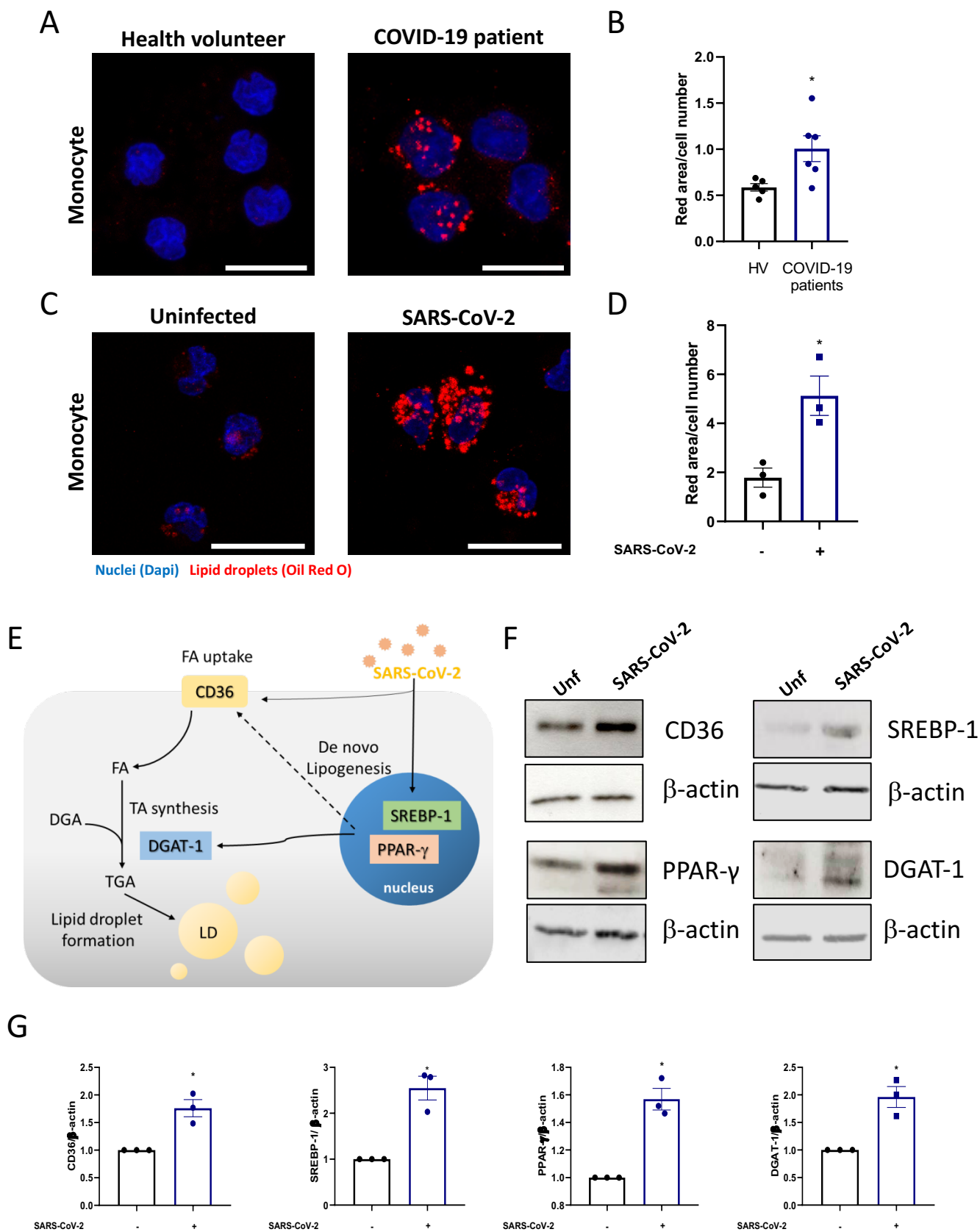


Figure 1

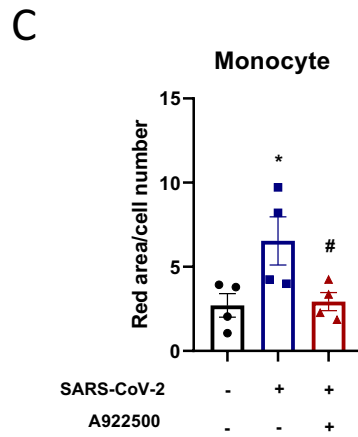
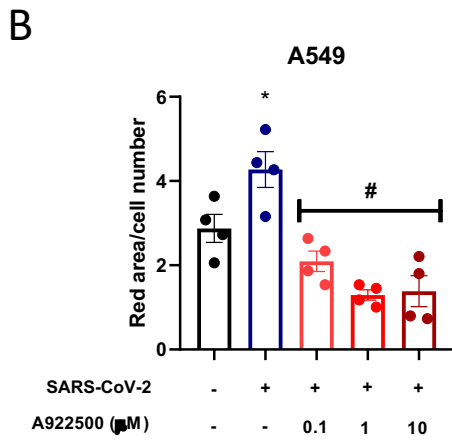
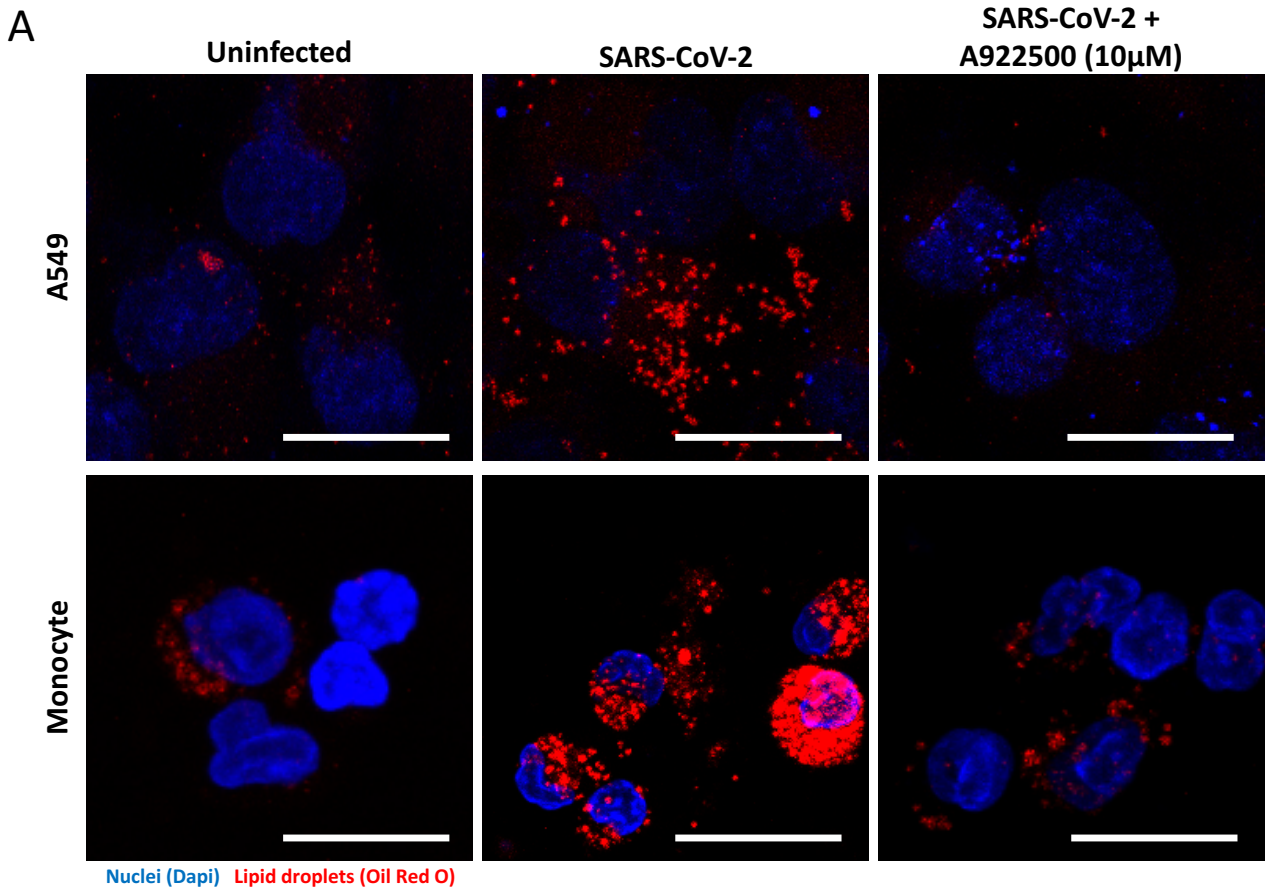


Figure 2

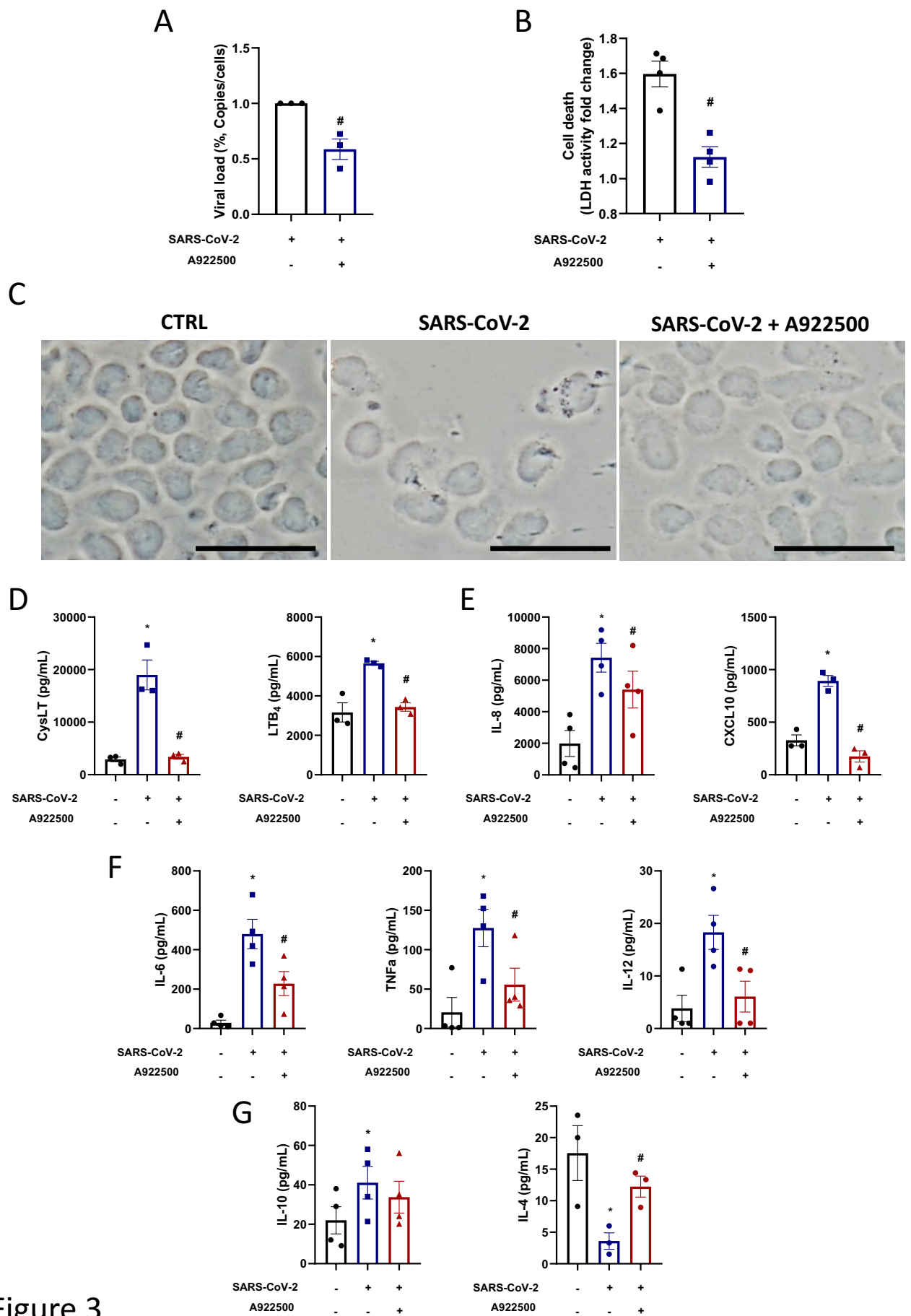


Figure 3



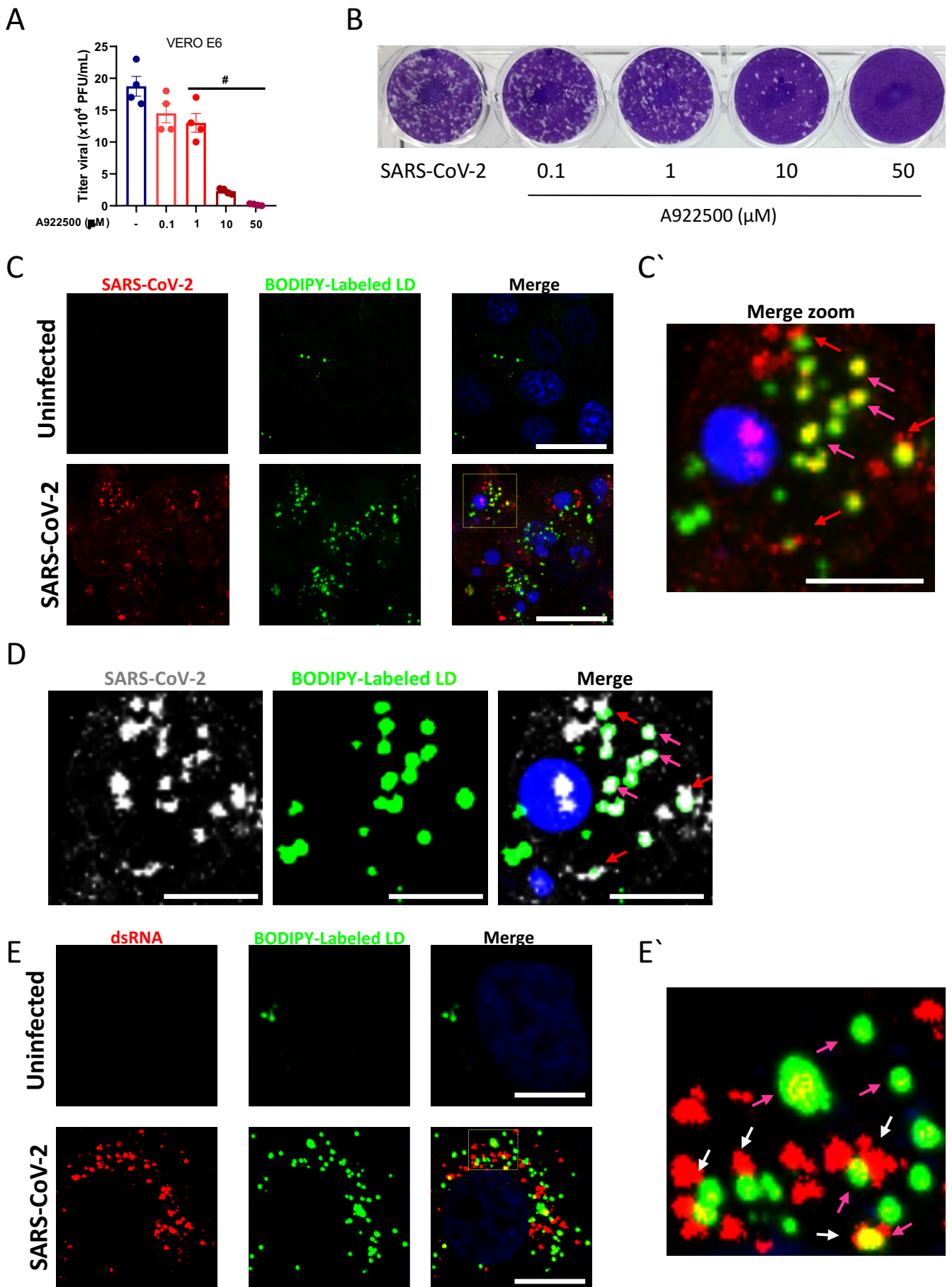
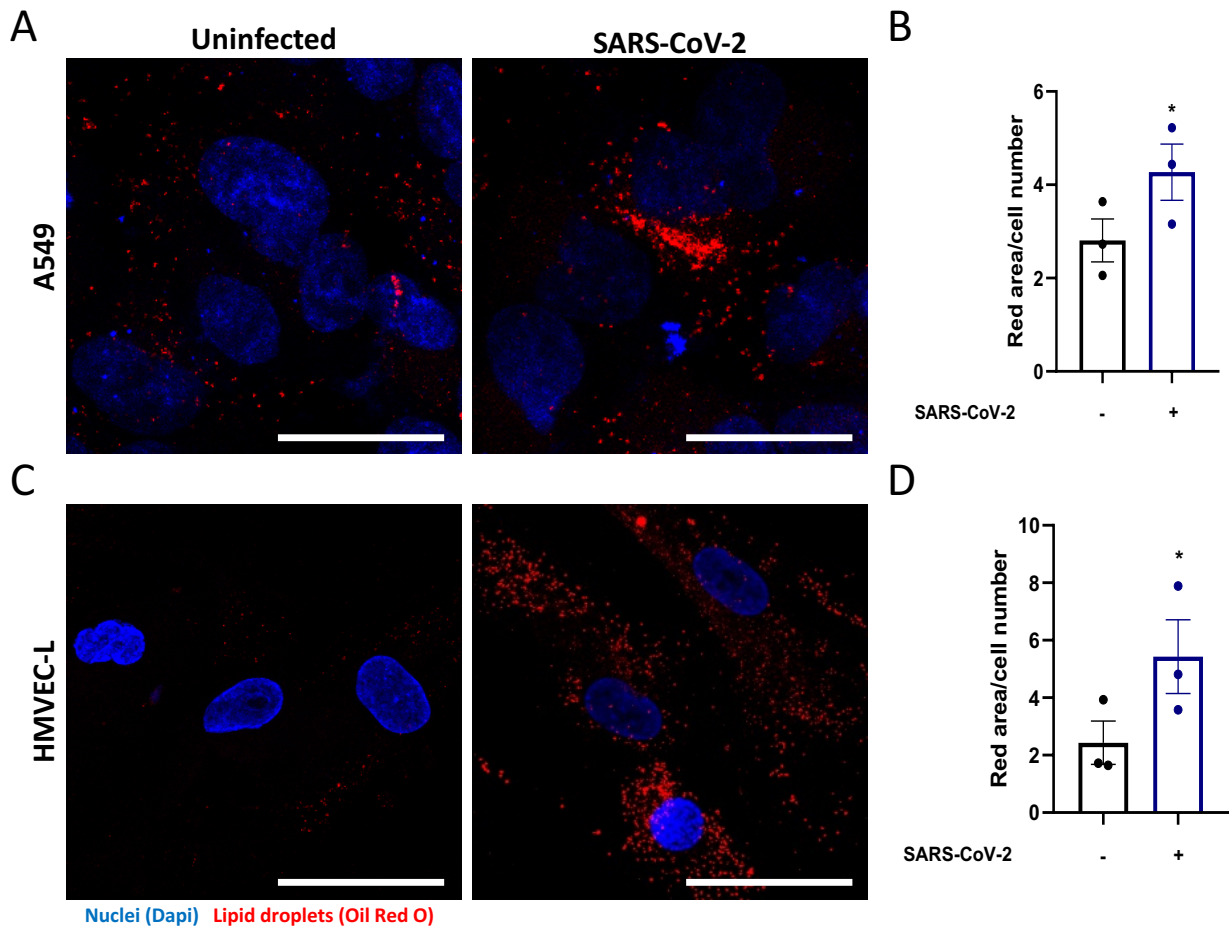


Figure 4



Supplementary Figure 1